Journal of The Electrochemical Society, **157** (5) A582-A588 (2010)
0013-4651/2010/157(5)/A582/7/$28.00 © The Electrochemical Society

Lithium Storage in Amorphous TiO_2 Nanoparticles

Wouter J. H. Borghols,[a,b] Dirk Lützenkirchen-Hecht,[c] Ullrich Haake,[c] Wingkee Chan,[a] Ugo Lafont,[d] Erik M. Kelder,[d] Ernst R. H. van Eck,[e] Arno P. M. Kentgens,[e] Fokko M. Mulder,[a] and Marnix Wagemaker[a,z]

[a]*RID, Faculty of Applied Sciences, Delft University of Technology, 2629JB Delft, The Netherlands*
[b]*Institut für Festkörperforschung, Forschungszentrum Jülich GmbH, Jülich Centre for Neutron Science at FRM II, 85747 Garching, Germany*
[c]*Fachbereich C-Physik, Bergische Universität Wuppertal, D-42097 Wuppertal, Germany*
[d]*DCT, Faculty of Applied Sciences, Delft University of Technology, 2628BL Delft, The Netherlands*
[e]*Solid State NMR, Institute for Molecules and Materials, Radboud University Nijmegen, Toernooiveld 1, 6525 ED Nijmegen, The Netherlands*

Amorphous titanium oxide nanoparticles were prepared from titanium isopropoxide. In situ measurements reveal an extraordinary high capacity of 810 mAh/g on the first discharge. Upon cycling at a charge/discharge rate of 33.5 mA/g, this capacity gradually decreases to 200 mAh/g after 50 cycles. The origin of this fading was investigated using X-ray absorption spectroscopy and solid-state nuclear magnetic resonance. These measurements reveal that a large fraction of the total amount of the consumed Li atoms is due to the reaction of H_2O/OH species adsorbed at the surface to Li_2O, explaining the irreversible capacity loss. The reversible capacity of the bulk, leading to the $Li_{0.5}TiO_2$ composition, does not explain the relatively large reversible capacity, implying that part of Li_2O at the TiO_2 surface may be reversible. The high reversible capacity, also at large (dis)charge rates up to 3.35 A/g (10C), makes this amorphous titanium oxide material suitable as a low cost electrode material in a high power battery.
 [DOI: 10.1149/1.3332806]

Manuscript submitted November 13, 2009; revised manuscript received January 26, 2010. Published April 7, 2010.

Electrochemical storage devices based upon lithium-ion technology have replaced earlier battery types in numerous applications, e.g., portable devices, mainly due to their high energy density, long cycle life, and their relatively low impact on the environment. If materials that support higher current densities during discharging and satisfy the safety issues concerned, Li-ion batteries would become available for heavy duty applications such as (hybrid) electrical cars.

A high power density requires both good ionic and electronic transport properties of the electrode materials. In many cases, the solid-state diffusion of Li ions through the electrode materials is several orders of magnitude smaller than in the electrolyte. Therefore, if the power density is to be improved, the electrode performance is to be investigated. In commercially available Li-ion batteries, the electrode material is dispersed in the electrolyte as microsized crystallites, which are capable of hosting the lithium ions inside their crystalline voids. By simply decreasing the size of these crystallites, the electrode–electrolyte interface is increased, whereas the diffusion length inside the electrode crystallite decreases. However, recent studies reveal a more complex behavior of nanosized Li insertion compounds in, e.g., TiO_2 anatase,[1-3] TiO_2 rutile,[4,5] or Li_xFePO_4,[6] showing distinct changes in electronic structure and ionic mobility upon downsizing to the nanodomain.[7] Usually, these differences in electronic structure and ionic mobility between bulk and nanosized crystallites are ascribed to the relatively increased impact of surface phenomena.[8-10] Between the crystalline structures anatase and rutile TiO_2, similarities were observed in the physical behavior of the nanoscale compounds. Both reveal an increased Li-ion capacity compared to their microscale counterparts, which appears to be facilitated by an anomalous phase behavior that is induced by the nanoscale.[2,5] The enhanced Li capacity of both structures is confirmed by electrochemical experiments, and, in addition, these studies suggest a decrease in Li-ion mobility because the capacity decreases as the dis(charge) rate increases.[4,11]

Several other polymorphs of TiO_2 are also reported to store Li ions, such as hollandite,[8] ramsdellite,[9] TiO_2(B),[10] and amorphous TiO_2,[11] but the most abundant morphologies of anatase and rutile are the most widely studied materials.

Here, we explore the lithium insertion and extraction in nanoscale amorphous TiO_2. Aiming at a complete understanding, we have, in addition to standard electrochemical (dis)charging, applied several microscopic and macroscopic probes including neutron diffraction (ND), X-ray absorption spectroscopy (XAS), ^{7}Li nuclear magnetic resonance (NMR), energy-dispersive spectroscopy (EDS), and thermogravimetric analysis (TGA). This has led to a consistent picture of the performance of this material revealing amorphous TiO_2 as a very promising candidate for cheap, high power, and high capacity anodes in Li-ion batteries.

Methods

Sample preparation.— Titanium isopropoxide, obtained from Aldrich, was mixed with demineralized water. The resulting white precipitate was filtered and subsequently washed with ethanol several times. This material is referred to as pristine amorphous TiO_2 (PA-TiO_2). This PA-TiO_2 is left to dry inside a vacuum oven at 400 K for a week. This vacuum-dried TiO_2 is referred to as VD-TiO_2. The chemically lithiated amorphous sample was prepared by first dispersing the VD-TiO_2 in hexane (anhydrous 95 + %, Aldrich), after which an excess *n*-butyllithium (1.6 M Aldrich)[12,13] was slowly added while stirring the mixture. This method allows insertion of lithium in a chemical way by an electrochemical driving force. To avoid lithium from reacting directly with air and moisture, the procedure was performed in a glove box under argon atmosphere having less than 1 ppm O_2 and moisture, both responsible for the formation of Li_2O, LiOH, Li carbonates, and Li nitrates[14] as potential impurities. The resulting Li mole fraction inside the amorphous host was determined by wet chemical inductively coupled plasma (ICP) spectroscopy, and the atomic percentages of Ti and O were obtained by EDS during transmission electron microscopy (TEM) measurements (Philips CM30T). The TGA data were recorded using a Perkin-Elmer TGA 7 thermogravimetric analyzer.

Neutron Diffraction.— The room temperature ND measurements were performed at POLARIS and the medium resolution, high intensity time-of-flight diffractometer at the ISIS pulsed neutron source (Rutherford Appleton Laboratory, U.K.). POLARIS is equipped with 434 detectors in 4 banks, covering angles between approximately 160° (backward scattering) and 13° (forward scattering). Both the pristine and lithiated samples were loaded in an argon atmosphere into airtight vanadium sample containers sealed with indium O-rings. The resulting ND patterns were refined using the

[z] E-mail: m.wagemaker@tudelft.nl

Rietveld method implemented in General Structure Analysis System (GSAS).[15] The d-spacing under consideration ranged from 0.3 to 4 Å.

Electrochemistry.— Electrodes were prepared from a slurry of VD-TiO_2, carbon black, and poly(vinylidene fluoride) with a composition of 70/20/10 wt % dispersed in *n*-methyl pyrrolidone and casted on an aluminum foil used as a current collector. Circular disks were punched out and placed in a coin cell with lithium as counter and reference electrodes. The electrolyte used was $LiPF_6$ in ethylene carbonate (EC)/dimethyl carbonate (DMC) (2:1). Charge/discharge tests were performed with an MACCOR S4000 cycler.

X-ray absorption.— The transmission mode experiments were performed at the X-ray undulator beamline BW1 and the bending magnet station E4 at the DORIS III storage ring at HASYLAB (Hamburg, Germany), operating at a positron energy of 4.45 GeV with approximately 100–150 mA of stored current. A double-crystal monochromator with two flat Si(111) crystals was used. X-ray absorption near-end structure (XANES) and extended X-ray absorption fine structure (EXAFS) data were collected at the Ti K edge (~4966 eV) at room temperature using N_2-filled ionization chambers as detectors for the incoming and transmitted intensities. A Ti metal foil was simultaneously investigated in parallel to the actual sample for the calibration of the energy scale. Before the experiments, the air-sensitive samples were sealed in a sample carrier with 7.6 μm Kapton foil windows within the glove box. Several Ti–O reference compounds with known structure and chemical valence such as TiO, Ti_2O_3, crystalline $Li_{0.5}TiO_2$, as well as anatase and rutile TiO_2 were evaluated for comparison.

Solid-state ^{7}Li NMR spectroscopy.— The ^{7}Li magic angle spinning (MAS) NMR (I = 3/2, 92.6% abundance) spectra were recorded on a Chemagnetics 600 Infinity (B_0 = 14.1 T) operating at 233.2 MHz. Each air-sensitive sample was first loaded in a vacuum-dried Teflon tube and sealed with cyanic acrylate glue, after which this assembly was mounted into 3.2 mm airtight zirconium rotors. The MAS probe head achieved spinning speeds up to 18.5 kHz in a dry nitrogen atmosphere. Chemical shifts were referenced to a 0.1 M LiCl aqueous solution. The spectra were recorded after a 30° (at $2\omega_{rf}$) radio-frequency pulse applied with a recycle delay of 20 s. The 90° pulse length was 1.9 μs. The T_1 relaxation time was determined to be well below 2 s for all temperatures using a saturation recovery experiment. Therefore, a pulse delay of 10 s was sufficient for quantitative measurements.

Neutron Diffraction, EDS, and TGA

Nitrogen absorption experiments reveal a Brunauer, Emmett, and Teller (BET) surface area of 598 m^2/g. The large surface area leads to significant OH and H_2O adsorption at the TiO_2 surface. For the as-prepared material (PA-TiO_2) TGA up to 1000 K measures a total weight loss of 15% (see Fig. 1).

Further experiments during this research were all performed on materials VD at 400 K (VD-TiO_2) because higher temperatures lead to crystallization into the anatase and eventually into the rutile structure. For these materials, the TGA results still imply a 13% weight loss due to H_2O/OH species. This implies that the VD-TiO_2 material contains approximately 0.75 H_2O per TiO_2 unit, most likely residing at the materials surface.

The atomic composition of VD-TiO_2 was investigated through EDS, which shows that the compound contains 3.5 ± 0.5 oxygen atoms per titanium atom. This again points at H_2O/OH adsorption at the surface of the amorphous TiO_2 material, although it indicates more than 0.75 H_2O per TiO_2 unit.

A structural investigation of VD-TiO_2 has been performed by high resolution TEM, X-ray diffraction, and ND. From the TEM micrographs of VD-TiO_2 (Fig. 2), the typical particle size of the powder was estimated to be around 2–3 nm. In line with that, if dense spherical particles are assumed, the 598 m^2/g BET surface

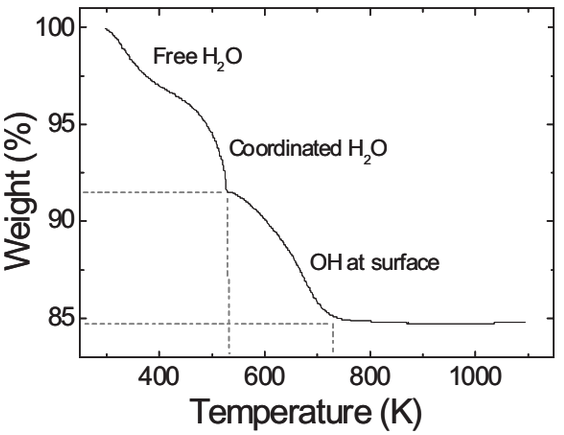

Figure 1. TGA of the as synthesized amorphous TiO_2 material.

corresponds to a typical size of ~2.5 nm particles. Assuming the anatase structure and the normally most abundant (101) surface orientation, this particle size implies that 54% of the Ti atoms are located near the particle surface. TEM also indicated a small amount of crystalline domains. The presence of crystalline phases was further investigated using X-ray and ND, the latter shown in Fig. 3 for both the VD-TiO_2 and the lithiated VD-TiO_2. The unlithiated material could be partially fitted with the anatase symmetry; however, other TiO_2 phases or a combination of various TiO_2 phases could not be excluded due to the large broadening of the reflections. No difference between the diffraction of the PA-TiO_2 (not shown) and VD-TiO_2 materials was detected, indicating that the crystalline fraction is formed during the synthesis, and no further crystallization occurs during the 400 K vacuum drying process. The large broadening and background confirm the TEM results that most of the material is amorphous with a minority of small crystalline domains, approximately 5%, assuming that all the background is due to the amorphous phase. Only small changes in the diffraction pattern occur upon lithiation, and the resulting pattern could be indexed and fitted reasonably well with the $Li_{0.5}TiO_2$ titanate, which forms from the lithiation of anatase TiO_2.[16,17] However, again, other phases can-

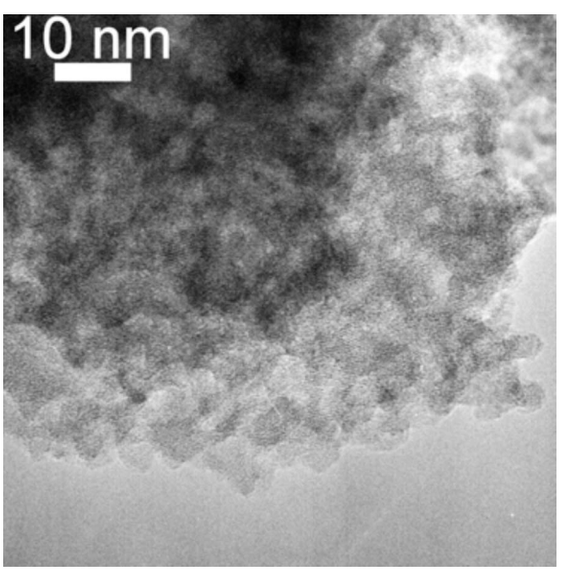

Figure 2. High resolution TEM micrograph of the VD-TiO_2 amorphous material.

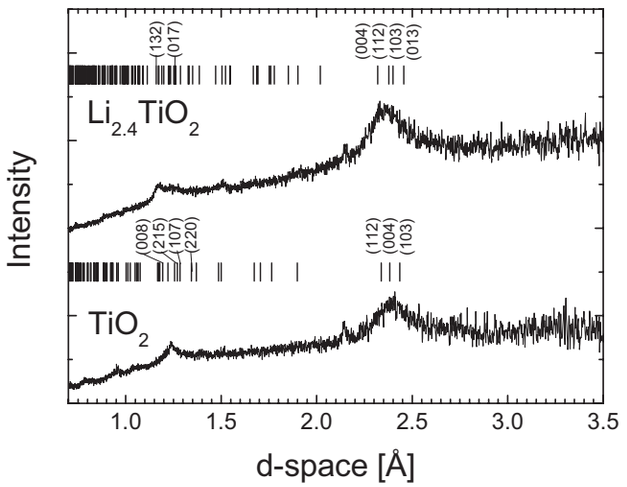

Figure 3. ND patterns of VD-amorphous TiO_2 (tick marks: TiO_2 anatase, space group $I4_1/amd$) and of the lithiated material (tick marks: $Li_{0.5}TiO_2$, space group *Imma*).

not be excluded due to the large broadening of the reflections. Nevertheless, it appears reasonable to assume that at least a part, approximately 5%, of the crystalline domains has a structure similar to anatase TiO_2.

Electrochemistry

The nanoscale or VD-TiO_2 was (dis)charged between 2.5 and 0.8 V, as shown in Fig. 4a. Typically, in the crystalline TiO_2 polymorphs, the maximum theoretical capacity is achieved when all possible crystal sites are occupied by Li ions. This situation is reached, having a composition of Li_1TiO_2 corresponding to a capacity of 335 mAh/g. In Fig. 4a, the galvanostatic test of VD-TiO_2 does not present a well-defined two-phase plateau in the first discharge. In the anatase TiO_2, this biphasic domain can be seen by the presence of a plateau around 1.78 V until a composition of $Li_{0.5-0.6}TiO_2$, both in micromaterials[18] as in nanomaterials.[19] In the first discharge in Fig. 4a, a small plateau at 1.78 V can be identified. The presence of this small plateau can be explained by a small percentage, roughly 9%, of a crystalline phase present in the sample, which is also observed in the TEM measurements on VD-TiO_2. Consistent with what was suggested by the diffraction in Fig. 3, this indicates a small fraction of anatase because this plateau ends at $Li_{0.55}TiO_2$, equal to the bulk anatase TiO_2.[18]

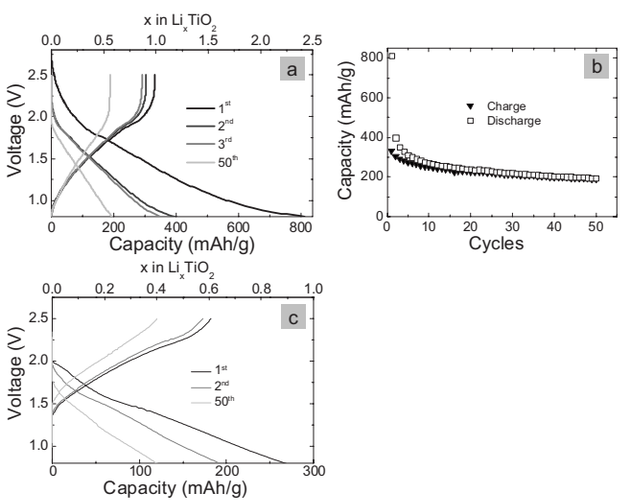

Figure 4. (a) The voltage profile of the test in galvanostatic mode (constant current) at C/10 (33.5 mA/g). (b) The degradation of capacity upon charge–discharge cycles. (c) The rechargeability of the amorphous TiO_2 electrode is investigated at a charge rate of 10C (3.35 A/g).

Using a charge/discharge current of 33.5 mA/g (C/10), VD-TiO_2 exhibits a very high specific capacity of 810 mAh/g during the first discharge to 0.80 V. This electrochemically obtained capacity corresponds to an unusually high composition of $Li_{2.4}TiO_2$, which agrees closely with the ICP measurements on chemically lithiated particles. To our knowledge, it is the highest specific capacity presented for titania based material so far. However, this extraordinary high capacity is not reversible because this specific capacity dramatically drops to 400 and 350 mAh/g for the second and third discharges, respectively. After 50 cycles, the discharge capacity appears to stabilize around 200 mAh/g.

An additional test was performed at a current rate of 3.35 A/g (10C), which is shown in Fig. 4c. Despite the high current, the material reached a specific capacity of 270 mAh/g. This capacity drops to 195 mAh/g at the end of the second discharge and reaches the value of ~125 mAh/g after the 50th discharge. The test at 10C shows a reversibility of ~120 mAh/g, which can be considered to be quite high compared to nanoscale anatase[19] and rutile,[4] which, at these higher power densities, both reach roughly 95 mAh/g. A reversible capacity of 120 mAh/g at 10C is comparable to TiO_2–B nanowires that show approximately 100 mAh/g [10] or TiO_2–B nanotubes at 100 mAh/g,[20] although both at a slightly lower rate of 6C. From the absence of distinct plateaus and the material's ability to accept this relatively high current density, it may be concluded that the lithium insertion in amorphous TiO_2 shows a typical solid solution behavior.

In summary, in the cycling experiments in Fig. 4a, three regions can be distinguished. First, a 50% loss in capacity is observed between the first and second cycles. Second, a gradual decrease in capacity between the 2nd and 50th cycles are obtained, and third, a reversible capacity of 200 mAh/g from the 50th cycle has been achieved. The remainder of this paper aims at understanding the (dis)charge behavior in more detail using XAS and NMR.

XAS

The electronic structures of VD-TiO_2 and chemically lithiated VD-TiO_2 are investigated using the Ti K edge XAS. The edge shift shown in the XANES spectrum in Fig. 5a of the untreated VD-TiO_2 compound is equal to the TiO_2 reference compound. The presence of Ti^{4+} indicates the amorphous material to have a TiO_2 composition. Therefore, the Ti/O ratio found by EDS, $1/(3.5 \pm 0.5)$, may indicate additional oxygen due to OH hydroxyl groups or H_2O molecules.

Upon Li insertion in VD-TiO_2, the edge position shifts to a lower energy by about 1.8 eV. This shift has been determined by the relative change in position of the maximum in the derivative spectra. In the inset of Fig. 5a, the edge shift is compared to the well-known shifts of several other titanium oxide reference compounds. Because the valence of Ti is well known for these reference samples, the Ti valence in lithiated VD-TiO_2 can be estimated from linear interpolation. This leads to a change in the Ti oxidation state from Ti^{4+} in VD-TiO_2 toward $Ti^{3.5+}$ in lithiated VD-TiO_2, i.e., $Li_{2.4}TiO_2$. The change in Ti valence, as determined from the observed relative edge shift, implies that only a fraction of about 0.5 Li 2s charge compensating electrons per TiO_2 formula unit influences the electronic properties at the Ti site, hence leading to a $Li_{0.5}TiO_2$ composition. This fraction agrees well with the fraction found in the (dis)charge measurements after the 50th cycle, i.e., the reversible part of the cycling measurements.

However, the first cycle of VD-TiO_2 revealed a fraction of 2.4 Li ions per TiO_2 formula unit, agreeing well with ICP measurements on the chemically lithiated material. Bearing in mind the decrease in the Ti valence from Ti^{4+} to $Ti^{3.5+}$, the comparison between the elec-

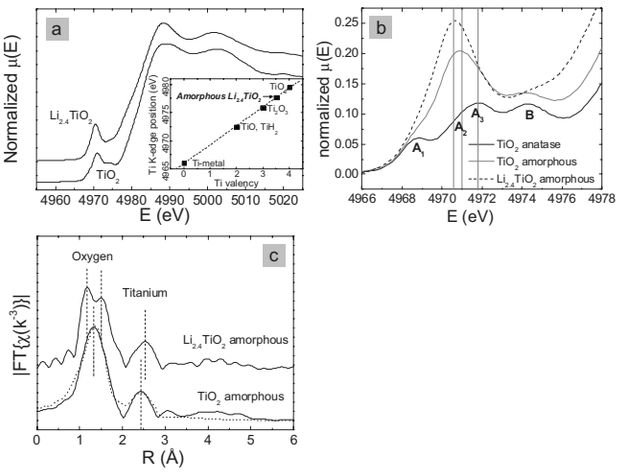

Figure 5. (a) XAS spectra of both VD-TiO_2 and lithiated VD-TiO_2, i.e., $Li_{2.4}TiO_2$. The inset shows a linear relationship between the edge position and the Ti valence. For comparison, the edge positions of $TiO_2(Ti^{4+})$, $Ti_2O_3(Ti^{3+})$, $TiO(Ti^{2+})$, and Ti metal (Ti^0) are also indicated. (b) Magnified view at the pre-edge features of VD-TiO_2 compared to the features in microcrystalline anatase TiO_2. (c) Magnitude of the Fourier transform of the experimental data and the results of an EXAFS fit result for the first two atomic shells surrounding the Ti atom.

trochemical results and ICP vs XANES leads to the conclusion that only 0.5 Li ions per TiO_2 unit out of the total 2.4 Li ions induce an electronic charge transfer toward the Ti atoms. Apparently, 1.9 Li ions (per TiO_2 unit) are stored in VD-TiO_2, in such a way that the average Ti valence is not influenced.

Figure 5b zooms in to the pre-edge features of the XAS spectra of VD-TiO_2 and lithiated VD-TiO_2. In Fig. 5b, TiO_2 anatase has been plotted as a reference compound. All three spectra have been aligned at the onset of the first absorption (~4967 eV). It is easily observed that the diversity of pre-edge features of anatase ($A_{1,2,3}$ and B) is more profound than in both VD-TiO_2 and lithiated VD-TiO_2, where at first glance, only a single absorption peak is observed. The physical reason for this is derived from the TiO_6 octahedron, which is present in all crystalline TiO_2 polymorphs, e.g., anatase, rutile, and brookite. In such an octahedral oxygen arrangement, the Ti 3d band is split into 3d-t_{2g} and 3d-e_g subbands due to the lowering in energy of the orbitals directed toward the oxygen atoms (3d-t_{2g} band, i.e., d_{xy}, d_{yz}, and d_{zx}) compared to the nondirectional orbitals (3d-e_g band, i.e., $d_{x^2-y^2}$ and d_{z^2}), a phenomenon referred to as "crystal-field splitting." For example, in anatase TiO_2, the $A_{2,3}$ prepeaks at ~4971 eV can be ascribed to the excitation of a Ti 1s electron to nondirectional Ti $3d(e_g)$ 4s hybridized states.

In both VD-TiO_2 and lithiated VD-TiO_2, this $A_{2,3}$ prepeak is strongly amplified compared to the A_1 and B peaks. This amplification of absorption peak $A_{2,3}$ strongly resembles the augmented peak found in anatase TiO_2 crystallites ~2 nm.[21] In this research, the increase in the intensity of the A_3 prepeak (there, the A_2 and A_3 peaks are both called A_2, although their A_3 peak is called B in our case) was assumed to be caused by the deformed oxygen octahedrons from regular TiO_6 to TiO_5 where one O has become larger Ti–O distance and effectively disappeared. Such situation is encountered at the surface of small powder particles. In our experiments, the amorphous sample could have this type of distortion throughout the bulk, proving this to be a truly irregular structure. It was shown by Farges et al.[22] that the coordination number of oxygen atoms surrounding the Ti atom is linearly correlated with both the pre-edge peak intensity and peak position of the A_3 absorption. For example, the average relative pre-edge peak height for a fivefold coordinated Ti site is three times that of a sixfold oxygen surrounding. Comparing the anatase pre-edge features to our pristine 25 Å amorphous particles, the latter pre-edge peak is about 1.6 times that of anatase. From this, we may estimate that about 60% of all Ti atoms experience fivefold oxygen coordination. The valence of Ti is 4+ in both the anatase TiO_6 octahedron and the distorted amorphous TiO_5 structure. The relative height of the A_{2-3} prepeak of the lithiated amorphous sample compared to anatase is ~2.5, which indicates a fraction of 90% of all Ti atoms to be pentacoordinated with oxygen.

A convincing argument for ascribing this reduction in coordination number to surface irregularities is given by Chen et al.[21] In this study, the authors managed to saturate the initial fivefold oxygen coordination to a full octahedron by allowing ascorbic acid to absorb to the surface. As a result, they found the A_3 prepeak to be lowered to the standard bulk anatase level because the initially shorter Ti = O double bond is broken and has reconnected with two hydroxyl oxygen atoms on the five member ring, forming two single Ti–O–(C) bonds. Upon increasing the coordination number of the Ti site from four to six oxygen atoms, the pre-edge intensity decreases and the energy of the peak increases by approximately 0.9 eV for each additional coordinating oxygen atom, starting from around 4969.6 eV for the tetrahedral Ti site. Our shift, as indicated by vertical lines in Fig. 5b, thus roughly corresponds to an oxygen coordination number of about 5.4.

In Fig. 5c, the EXAFS features of the PA-TiO_2 material are presented. Despite the absence of a well-defined crystalline symmetry in the amorphous material, some short-range ordering at the first and second atomic shells around titanium is expected. For this reason, the fit of the EXAFS spectrum has been performed by using TiO_2 anatase as the fit starting model because the local ordering of amorphous TiO_2 is similar to anatase.[23] From the fit results, the first peak(s) are ascribed to the Ti–O bond, and the second peak is ascribed to Ti–Ti bond. In the PA sample, the first shell of oxygen atoms appears to have a coordination number of 5.4 ± 0.4 in the best fit. The $Li_{2.5}TiO_2$ sample shows a reduced total of 5.0 ± 0.4 oxygen coordination. Besides this lowering in oxygen coordination number, the distances between Ti and O appear to be distorted, as can be seen easily from the double peak arising in the oxygen EXAFS peak in the lithiated amorphous sample. Although the accuracy of this fit is quite poor in the absence of an amorphous model to fit these results to, it confirms the conclusions drawn from the pre-edge part of the XANES in the previous section, i.e., the presence of a reduced coordination number.

In conclusion, the oxygen coordination numbers for both pristine and chemically lithiated amorphous samples have been determined to be roughly 5.4 for the pristine and 5.0 for the lithiated amorphous sample. Because the pre-edge features of the amorphous samples still show some intensity at the A_1 prepeak, it is concluded that the overall $TiO_{5.4}$ comprises well-defined TiO_6 and TiO_5 units, leading to 60% TiO_5 and 40% TiO_6 units. This agrees well with the modeled assumption of TiO_6 in the bulk and TiO_5 at the surface,[24] whereas in our case, the approximately calculated 54% Ti atoms resides at the surface. The same reasoning applies for the lithiated sample, showing that all unit building blocks are TiO_5. Obviously, the change in basic building blocks upon Li insertion has been determined from the altered electronic conditions, and it is not assumed that a large amount of oxygen atoms vanished from TiO_2 toward $Li_{2.4}TiO_2$.

The overall Li fraction in the maximum lithiated amorphous TiO_2 structure is 2.4 Li/Ti; however, the edge shift indicates only a small fraction of 0.5 Li/Ti, which influences the Ti electronic structure. This corresponds to the reversible part in the electrochemistry. From XAS alone, we were not able to account for the remaining excess Li of 1.9 Li/Ti, although the degeneration of oxygen coordination may suggest a lithium–oxygen interaction at the surface.

MAS Analysis

In Fig. 6b, the temperature-dependent full MAS spectra of the fully lithiated material are shown, and in Fig. 6c, the center bands are shown. The center band reveals at least two Li environments, which at the highest temperature, can be fitted as follows (shown in

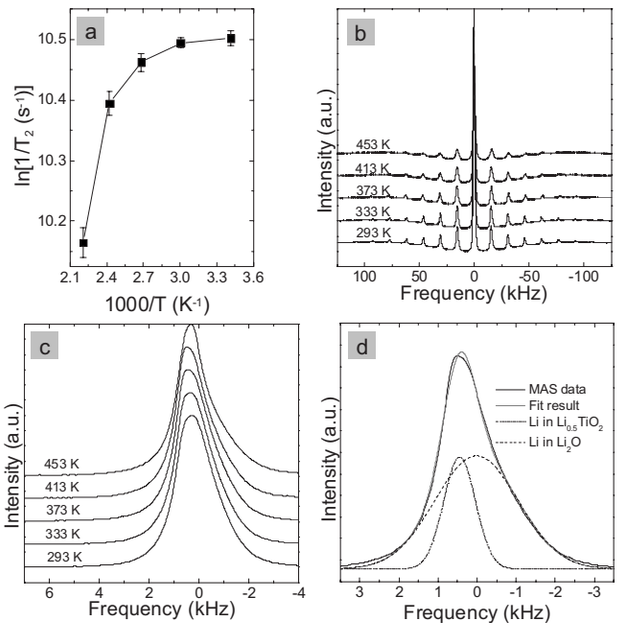

Figure 6. (a) Arrhenius plot of the ^{7}Li spin–spin relaxation time (T_2) for the maximum chemically lithiated amorphous $Li_{max}TiO_2$. The data were acquired under nonspinning conditions (Chemagnetics 600). (b) Full MAS spectra of the maximum lithiated amorphous $Li_{2.4}TiO_2$ at different temperatures. (c) Center band of the MAS spectra in (a). (d) Fit of the MAS center band at $T = 413$ K.

Fig. 6d); one that has a width of ~1.1 kHz (4.5 ppm) and a position of ~0.55 kHz (+2.3 ppm). This is not far from the values found for Li in 40 nm $Li_{0.72}TiO_2$ [1] at room temperature and one broader signal at ~0 ppm with an intensity that is about 2.5 times stronger in the center band. These signals might therefore be interpreted as resulting from Li in the nanoscale $TiO_{\sim 2}$-like fraction and the Li_2O-surface-like fraction of the material, where the intensity ratio is similar to what is discussed below in terms of the reversible respectively irreversible fraction of the stored Li in the material.

NMR: The Li-Ion Mobility Inside the Amorphous TiO_2 Host from T_2 Relaxation Measurements

The spontaneous mobility of the Li ions inside the TiO_2 amorphous structure was probed with static ^{7}Li NMR T_2 relaxation measurements. The T_2 relaxation time, a measure for the spin–spin interaction and spatial and temporal correlation, increases upon increasing Li-ion mobility through the lattice. The rise in T_2 causes the resonance in the frequency domain to become narrower, an effect that is referred to as motional narrowing. In this way, the T_2 relaxation time is a probe of the Li-ion mobility, and the knowledge of T_2 vs temperature allows the determination of the (self) diffusion coefficient and its activation energy, quantifying the time scale and the barrier for Li hopping, respectively, through the crystalline host lattice.[25,26]

If the mobility of the Li ions is assumed to be thermally activated, the spin–spin spatial correlation time obeys an Arrhenius law, $\tau_c = \tau_\infty \exp(E_A/k_B T)$, where E_A is the activation energy of the jump process and $1/\tau_\infty$ is the attempt frequency. From the increase in the T_2 value vs temperature in the Arrhenius plot shown in Fig. 6a, the Li-ion movement indeed appears thermally activated. From the slope of the linear fit of the high-T regime in the Arrhenius plot the activation energy can be determined. The value of $E_A = 0.16 \pm 0.03$ eV is fairly low, and it closely resembles the activation energy of lithium in the solid solution regime of bulk sized anatase (0.20 ± 0.01 eV).[25]

The XAS and MAS NMR results of the previous sections suggest more than one Li-ion environment in or at the surface of the amorphous structure, i.e., inserted Li ions influencing the Ti valence and the yet unidentified excess of 1.9 Li per formula unit. Although different Li environments would imply distinct T_2 signals, only one was identified; the static T_2 values in Fig. 6a are the result of fitting the T_2 relaxation data with a single exponential decay. In the work of Strange et al.,[27] T_2 relaxation times for pure, crystalline Li_2O are reported as ~40 μs at 300–400 K. This value is close to the T_2 value found here in the amorphous and nanostructured materials, and the same holds for the T_2 value in Li titanate.[1,25] Apparently, the T_2 of the amorphous material, although representing two contributions of different Li environments, only leads to one experimental static T_2 value. In both pure bulk Li_2O and Li titanate, the mobility increases when raising the temperature, where Li titanate shows the larger mobility. In the amorphous sample, no difference can be detected in the T_2 and hence the mobility of the different environments. This might be interpreted in several ways: The mobility is the same in different environments or there is an exchange in the T_2 time scale between the different environments, which leads to averaging and apparently a single experimental T_2. As can be expected from the time scale of the mobility at high temperatures, the mobility also has an effect on the MAS spectra in Fig. 6b: The sideband pattern becomes less wide, and the peaks broaden.

An estimate of the microscopic diffusion coefficient D at room temperature has been determined with $D = l^2/n\tau_c$, where l is the length of an elementary jump between sites and n is the number of possible jumps to different neighboring sites. Both parameters l and n cannot be accurately determined in the absence of a clear defined structure in the amorphous materials.

In anatase and rutile, where the basic building block of the structure is the oxygen octahedron, an equivalent Li site is found fourfold at about 3 Å. Although the XAS analysis indicates a deterioration of this sixfold oxygen coordination toward a fivefold, the length for Li hops is assumed to be the same. This should produce numbers that are relatively close to the true results. Then, the diffusion coefficient at room temperature results in $D = 3.5 \times 10^{-12}$ cm^2 s^{-1}. This is a relatively large diffusion coefficient, which, together with the nanoscale of the particles, can explain the relatively large reversible capacity found in the electrochemical tests performed at high charge rates (10C) because a high Li-ion mobility supports a high charge rate.

Discussion

Electrochemical experiments at a charge rate of C/10 on nanoscale TiO_2 amorphous (2.5 nm) have revealed a very large capacity of 810 mAg/h during the first discharge, leading to a composition of $Li_{2.4}TiO_2$. Because this result is confirmed by ICP measurements in the chemically lithiated material, the large Li fraction appears independent of the insertion method. The second charge cycle in the electrochemistry already shows a decrease in this capacity by about 50%, and from the 2nd to the 50th cycles, the capacity is decreased by another 50% to leave a recyclable capacity of about 200 mAg/h. Compared to other nanosized titanium oxides such as rutile (160 mAh/g),[4] anatase (190 mAh/g)[19] at the same charge rate of C/10, or TiO_2–B nanowires (180 mAh/g)[10] and nanotubes (220 mAh/g)[20] C/7, a reversible capacity of 200 mAh/g found in nanotextured amorphous TiO_2 is reasonably high.

The observed drop in Ti valence from Ti^{4+} to $Ti^{3.5+}$ in the XAS measurements indicates that only 0.5 Li per TiO_2 is actually inserted in the host. This fraction of 0.5 Li per TiO_2 is most likely responsible for the large part of the reversible capacity after the 50th cycle. The remaining 1.9 Li per TiO_2 unit atoms is irreversibly lost after the first discharges. The reversible capacity is 200 mAh/g, whereas the capacity of 0.5 Li per TiO_2 is only 130 mAh/g (taking the H_2O and OH content into account; see below). Hence, part of the reversible capacity must be due to some sort of surface reaction. The first option that should be considered is the irreversible capacity loss due

to solid electrolyte interphase (SEI) formation. However, for similar large-area titanium oxides, SEI formation occurs around 0.8 V and is basically absent above 1 V.[20,28] Therefore, we expect only a small fraction of the irreversible capacity to be due to SEI formation.

Titanium dioxide surfaces are well known to adsorb H_2O and OH both physically and chemically. Therefore, in particular, during the first cycles, Li ions may be expected to react with these adsorbed species to Li_2O, which may be expected to be irreversible in the applied voltage window. The presence of Li_2O indeed appears to be confirmed by the ^7Li NMR experiments. Li_2O is a good ionic conductor,[29] and, therefore, it may not lead to a large barrier Li transport.

The formation of Li_2O at the TiO_2 surface suggests that the H_2O/OH groups present at the surface have their H replaced. In chemical lithiation with *n*-butyllithium, we propose the following reaction (which is quite well known for butyllithium)

$$TiO_2(H_2O)_x + (0.5 + 2x)LiC_4H_9(n\text{-}BuLi) \rightarrow Li_{0.5}TiO_2 + xLi_2O(\text{surface}) + 2xC_4H_{10} + 0.5C_4H_9 \quad [1]$$

Because butyl is not a stable reaction product, butane either reacts to octane ($0.5C_4H_9 \rightarrow 0.25C_8H_{18}$) or disproportionate to a combination of butane and butene ($0.5C_4H_9 \rightarrow 0.25C_4H_{10+}0.25C_4H_8$). A similar reaction can be written down for the reaction with OH. The rest product of the reaction is thus a mixture of butane and butene or octane. In this reaction, hydrogen released from H_2O at the surface has reacted with butyllithium to form butane.

Also in the electrochemical (dis)charging conditions, with the presence of the electrolyte, $LiPF_6$ in EC/DMC (2:1), the proposed formation of Li_2O at the surface implies dehydrogenation of the surface. A possible exothermic reaction that can occur in the presence of a catalyst is the formation of ethylene glycol and carbonmonoxide.[30] The formation of Li_2O at the TiO_2 surface would proceed as follows

$$2TiO_2(H_2O)_x + (1 + 4x)Li + 2xC_2H_4O_2CO(EC) \rightarrow 2Li_{0.5}TiO_2 + 2xLi_2O + 2xC_2H_4(OH)_2 + 2xCO \quad [2]$$

A similar reaction can be written down for the reaction with OH, where CO may react with Li^+ ions in the electrolyte toward Li carbonyl complexes.[31]

The pre-edge features of the XAS spectra have revealed that the pristine and lithiated amorphous structures are both built up of TiO_6 octahedrons and TiO_5 structures. As may be expected, the fivefold coordinated Ti atoms are present at the surface,[21] offering suitable adsorption sites, assuming that the surface of the amorphous is similar to the anatase surface.[32] To estimate the irreversible capacity by the formation of Li_2O due to the presence of H_2O and OH at the TiO_2 surface, we assume for simplicity that the surface of the amorphous material is similar to the anatase surface, which is dominated by the (101) and (100)/(010) surfaces. On these surfaces, water is absorbed dominantly in a molecular state rather than as hydroxyl groups.[32-34] Adsorption energies on the available fivefold coordinated Ti atoms on the 101 surface H_2O values are experimentally found to be between 0.5 and 0.7 eV,[35] and 0.7 eV by DFT which appears largely independent of the coverage.[32] Such large adsorption energies indicate that weight loss during the TGA measurements is most likely not due to the desorption of these strongly bound H_2O molecules but rather due weakly bound H_2O and OH at the surface of the particles. The Ti–OH_2 bond length was calculated to be 2.28 Å,[32] whereas the typical octahedral environment of the Ti–O bond is approximately 1.9 Å. Therefore, a coordination number of Ti between 5 and 6 may be expected, which is confirmed by the 5.4 coordination found by EXAFS and XANES. If we assume that a reaction with Li ions leads to the Li_2O end product, we can simplify the calculation by assuming that only H_2O molecules are absorbed. Assuming that all available fivefold coordinated Ti atoms host one H_2O molecule (strongly bound, not observed by TGA) and assuming the specific surface area to be 598 m^2/g (from BET), this leads to only 0.54 H_2O per TiO_2 formula unit (Ti/O ratio 1/2.54), whereas EDS indicates 1.5 ± 0.5 H_2O per TiO_2 formula unit (Ti/O ratio 1/3.5). If we consider the H_2O detected by TGA, which shows 13% weight loss from a VD material at 373 K, referred to as weakly bound H_2O/OH, this accounts roughly for an additional 0.75 H_2O per TiO_2 formula unit. Taking both strongly and weakly bound H_2O contributions into account, this leads to 1.3 H_2O per TiO_2 formula units (Ti/O ratio 1/3.3), which agrees well with the EDS results.

Table I. Specific capacities calculated based on Li insertion in the amorphous TiO_2 host and formation of Li_2O from surface adsorbed H_2O, both strongly bound and weakly bound.

Composition	Specific capacity (mAh/g)
$Li_{0.5}TiO_2$:$(H_2O)_{1.29}$	130
TiO_2:$(H_2O)_{0.54}$:$(Li_2O)_{0.75}$	390
TiO_2:$(Li_2O)_{0.54}$:$(H_2O)_{0.75}$	281
$Li_{0.5}TiO_2$:$(Li_2O)_{1.29}$	801

Based on this H_2O capacity, and assuming all hydrogen ions are replaced by Li ions during the chemical and electrochemical lithiation, in addition to the Li-ion insertion, we can calculate the expected capacities (see Table I).

The total capacity, where all adsorbed H_2O is reacted to Li_2O, is remarkably close to the capacity found for the first discharge (810 mAh/g). Although no value should be given to the exact number, the fact that the order of magnitude is correct argues for the proposed reaction of H_2O/OH adsorbed at the TiO_2 surface toward Li_2O. The formation of Li_2O may be expected to be largely irreversible, explaining the large irreversible capacity. Nevertheless, the reversible formation of just $Li_{0.5}TiO_2$ is insufficient to explain the observed 200 mAh/g reversible capacity after 50 cycles. Hence, we propose that part of this capacity may be due to reversible storage in the form of Li_2O at the TiO_2 surface. Clearly, this $2xLi_2O$ on TiO_2 from Eq. 2 needs to form a TiO_{2+x} composition upon reversible Li extraction, possibly resulting in titanium peroxide (predominantly at the surface). Different titanium peroxides are known to exist,[36,37] in which effectively peroxo groups O_2^{2-} are present. The reversible reduction of these O_2^{2-} groups by the addition of Li may be the mechanism that explains the reversible surface storage. An overall equation for such reversible reaction would be as follows

$$[Li_{0.5}TiO_2 + xLi_2O] \rightarrow [TiO_{2+x}] + Li_{0.5+2x} \quad [3]$$

where the brackets indicate that the reactants form a single few nanometer particle consisting of an $\sim TiO_2$ core and an oxygen-rich surface. At this stage, we do not understand how the formation of Li_2O at the TiO_2 surface decreases the Ti–O coordination from 5.4 in TiO_2:$(H_2O)_{1.29}$ to 5.0 in $Li_{0.5}TiO_2$:$(Li_2O)_{1.29}$, as observed by XANES (Fig. 5b) and EXAFS (Fig. 5c) results. This may be either due to a change in the Ti–O coordination in the bulk of the material or due to the different nature of the bonding of Li_2O to the TiO_2 surface compared to H_2O. In bulk anatase, the formation of $Li_{0.5}TiO_2$ leads to the splitting of the first Ti–O coordination shell, which, in the more disordered amorphous compound, may appear effectively as a reduction of the Ti–O coordination. Presently, detailed knowledge of Li_2O on transition-metal oxides appears largely unavailable, although it appears very relevant for Li-ion battery electrodes.

The reversible formation of Li_2O is well known for several nanosized transition-metal oxides;[38] however, in that case, the storage mechanism involves the decomposition of metal oxides and the formation of Li_2O during Li insertion and the reformation of the metal oxides on extraction. Although such conversion reactions do not appear to exist for titanium oxides at present, we speculate possible reversible formation of a small fraction of Li_2O at the surface of amorphous TiO_2. Such reversible capacity would offer interesting

possibilities for cheap high capacity, high power anode materials for Li-ion batteries; however, more research is required to establish this phenomena.

In general, nano-titanium oxides appear to behave very similarly, showing a large initial capacity that scales with the surface area and appears largely irreversible.[4,5,39,40,10,20] At similar voltages, a comparable large irreversible capacity loss during the first cycles was observed in TiO_2–B, which is also prepared in a water-rich environment.[10,20] Because no significant SEI formation was detected, it was suggested to be the consequence of poor electronic conductivity due to Li depletion at the near-surface region. The present results offer an alternative explanation based on the always present H_2O/OH surface adsorbed species.

Conclusions

Nanostructured amorphous TiO_2 leads to a very high discharge capacity of 810 mAg/h in the first cycle. However, only ~25% of the capacity appears to be reversible after 50 cycles. Nevertheless, the nanoscale amorphous titanium oxide remains to have a high reversible capacity compared to other titanium oxide morphologies, especially at a higher charge rate of 3.35 A/g (10C). The change in Ti valence, observed by XAS, explains only a part (130 mAh/g) of the reversible and irreversible capacities. The presence of adsorbed H_2O/OH species at the TiO_2 surface leads to the formation of Li_2O, as observed by ^{7}Li NMR, which explains the large irreversible capacity. Part of the Li_2O at the TiO_2 surface must be reversible to explain the relatively large reversible capacity of 200 mAh/g, possibly due to the formation of Ti peroxide at the particle surface. This phenomenon, in addition to the large (dis)charge capacity at large (dis)charge rates, makes these materials very appealing for cheap, high rate, high capacity Li-ion anodes.

Acknowledgments

We thank HASYLAB for the provision of beam time and the financial support of our experiments and D. Zajac and D. Novikov for their excellent support at the beam lines. The financial support from the Netherlands Organization for Scientific Research (NWO) for the VIDI grant of M.W. is gratefully acknowledged. NWO is further acknowledged for financing the solid-state NMR facility for advanced material science at the Radboud University. We thank the Alistore network for providing access to TEM measurements and the electrochemical laboratories.

Delft University of Technology assisted in meeting the publication costs of this article.

References

1. M. Wagemaker, W. J. H. Borghols, E. R. H. van Eck, A. P. M. Kentgens, G. J. Kearley, and F. M. Mulder, *Chemistry (Weinheim, Ger.)*, **13**, 2023 (2007).
2. M. Wagemaker, W. J. H. Borghols, and F. M. Mulder, *J. Am. Chem. Soc.*, **129**, 4323 (2007).
3. W. J. H. Borghols, D. Lutzenkirchen-Hecht, U. Haake, E. R. H. van Eck, F. M. Mulder, and M. Wagemaker, *Phys. Chem. Chem. Phys.*, **11**, 5742 (2009).
4. Y. S. Hu, L. Kienle, Y. G. Guo, and J. Maier, *Adv. Mater.*, **18**, 1421 (2006).
5. W. J. H. Borghols, M. Wagemaker, U. Lafont, E. M. Kelder, and F. M. Mulder, *Chem. Mater.*, **20**, 2949 (2008).
6. N. Meethong, H. Y. S. Huang, W. C. Carter, and Y. M. Chiang, *Electrochem. Solid-State Lett.*, **10**, A134 (2007).
7. A. S. Aricò, P. Bruce, B. Scrosati, J. M. Tarascon, and W. Van Schalkwijk, *Nature Mater.*, **4**, 366 (2005).
8. L. D. Noailles, C. S. Johnson, J. T. Vaughey, and M. M. Thackeray, *J. Power Sources*, **81–82**, 259 (1999).
9. A. Kuhn, R. Amandi, and F. Garcia-Alvarado, *J. Power Sources*, **92**, 221 (2001).
10. A. R. Armstrong, G. Armstrong, J. Canales, R. Garcia, and P. G. Bruce, *Adv. Mater.*, **17**, 862 (2005).
11. M. Hibino, K. Abe, M. Mochizuki, and M. Miyayama, *J. Power Sources*, **126**, 139 (2004).
12. M. S. Whittingham and M. B. Dines, *J. Electrochem. Soc.*, **124**, 1387 (1977).
13. R. R. Ernst, G. Bodenhausen, and A. Wokaun, *Principles of Nuclear Magnetic Resonance in One and Two Dimensions*, Clarendon, Oxford (1994).
14. S. Södergren, H. Siegbahn, H. Rensmo, H. Lindström, A. Hagfeldt, and S.-E. Lindquist, *J. Phys. Chem. B*, **101**, 3087 (1997).
15. W. G. Williams, R. M. Ibberson, P. Day, and J. E. Enderby, *Physica B*, **241–243**, 234 (1997).
16. R. J. Cava, D. W. Murphy, S. Zahurak, A. Santoro, and R. S. Roth, *J. Solid State Chem.*, **53**, 64 (1984).
17. M. Wagemaker, G. J. Kearley, A. A. van Well, H. Mutka, and F. M. Mulder, *J. Am. Chem. Soc.*, **125**, 840 (2003).
18. W. J. Macklin and R. J. Neat, *Solid State Ionics*, **53–56**, 694 (1992).
19. C. H. Jiang, M. D. Wei, Z. M. Qi, T. Kudo, I. Honma, and H. S. Zhou, *J. Power Sources*, **166**, 239 (2007).
20. G. Armstrong, A. R Armstrong, J. Canales, and P. G. Bruce, *Electrochem. Solid-State Lett.*, **9**, A139 (2006).
21. L. X. Chen, T. Rajh, J. Nedeljkovic, and M. C. Thurnauer, *J. Synchrotron Radiat.*, **6**, 445 (1999).
22. F. Farges, G. E. Brown, and J. J. Rehr, *Phys. Rev. B*, **56**, 1809 (1997).
23. M. Strømme, R. Ahuja, and G. A. Niklasson, *Phys. Rev. Lett.*, **93**, 206403 (2004).
24. V. V. Hoang, H. Zung, and N. H. B. Trong, *Eur. Phys. J. D*, **44**, 515 (2007).
25. M. Wagemaker, R. van de Krol, A. P. M. Kentgens, A. A. van Well, and F. M. Mulder, *J. Am. Chem. Soc.*, **123**, 11454 (2001).
26. N. Bloembergen, E. M. Purcell, and R. V. Pound, *Phys. Rev.*, **73**, 679 (1948).
27. J. H. Strange, S. M. Rageb, A. V. Chadwick, K. W. Flack, and J. H. Harding, *J. Chem. Soc., Faraday Trans.*, **86**, 1239 (1990).
28. W. J. H. Borghols, U. Laffont, E. M. Kelder, F. M. Mulder, and M. Wagemaker, *J. Am. Chem. Soc.*, **131**, 17786 (2009).
29. A. V. Chadwick, K. W. Flack, and J. H. Strange, *Solid State Ionics*, **28–30**, 185 (1988).
30. K. I. Tominaga, Y. Sasaki, T. Watanabe, and M. Saito, *J. Chem. Soc., Chem. Commun.*, **1995**, 1489.
31. B. Silvi, O. Ayed, and W. B. Person, *J. Am. Chem. Soc.*, **108**, 8148 (1986).
32. A. Vittadini, A. Selloni, F. P. Rotzinger, and M. Gratzel, *Phys. Rev. Lett.*, **81**, 2954 (1998).
33. K. I. Hadjiivanov and D. G. Klissurski, *Chem. Soc. Rev.*, **1996**, 61.
34. D. D. Beck, J. M. White, and C. T. Ratcliffe, *J. Phys. Chem.*, **90**, 3123 (1986).
35. M. Egashira, S. Kawasumi, S. Kagawa, and T. Seiyama, *Bull. Chem. Soc. Jpn.*, **51**, 3144 (1978).
36. G. Schwarzenbach, J. Muehlebach, and K. Mueller, *Inorg. Chem.*, **9**, 2381 (1970).
37. G. V. Jere and C. C. Patel, *Z. Anorg. Allg. Chem.*, **319**, 175 (1962).
38. P. Poizot, S. Laruelle, S. Grugeon, L. Dupont, and J. M. Tarascon, *Nature (London)*, **407**, 496 (2000).
39. J. Jamnik and J. Maier, *Phys. Chem. Chem. Phys.*, **5**, 5215 (2003).
40. G. Sudant, E. Baudrin, D. Larcher, and J. M. Tarascon, *J. Mater. Chem.*, **15**, 1263 (2005).